	<p>Scientific and Validation Report for the “Automatic Satellite Image Interpretation – Next Generation” Processors of the NWC/GEO</p>	<p>Code: NWC/CDOP4/MTG/GSA/SCI/VR/ASII-NG Issue: 1.0.0 Date: 31 March 2025 File: NWC-CDOP4-MTG-GSA-SCI-VR-ASII-NG_v1.0.0 Page: 1/24</p>
---	--	--



Scientific and Validation Report for the “Automatic Satellite Image Interpretation – Next Generation” Processors of the NWC/GEO

NWC/CDOP4/MTG/GSA/SCI/VR/ASII-NG, Issue 1.0.0

31 March 2025

Applicable to

GEO-ASII-NG-v3.0 (NWC-049)

which is comprised of

GEO-ASII-TF-v3.0


GEO-ASII-GW-v2.0

GEO-ASII-ICE-v1.0

Prepared by GeoSphere Austria

REPORT SIGNATURE TABLE

Function	Name	Signature	Date
Prepared by	A. Jann (GSA) for ASII-GW and ASII-ICE, A. Wirth (GSA) for ASII-TF		31 March 2025
Reviewed by	P. Schmederer (GSA), plus: A. Jann (GSA) for ASII-TF, A. Wirth (GSA) for ASII-GW and ASII-ICE		31 March 2025
Authorised by	Pilar Ripodas, AEMET SAFNWC Project Manager		31 March 2025

	<p>Scientific and Validation Report for the “Automatic Satellite Image Interpretation – Next Generation” Processors of the NWC/GEO</p>	<p>Code: NWC/CDOP4/MTG/GSA/SCI/VR/ASII-NG Issue: 1.0.0 Date: 31 March 2025 File: NWC-CDOP4-MTG-GSA-SCI-VR-ASII-NG_v1.0.0 Page: 3/24</p>
---	--	---

DOCUMENT CHANGE RECORD

Version	Date	Pages	CHANGE(S)
1.0.0	31 March 2025	24	First CDOP-4 version, for the first MTG release

Table of contents

1. INTRODUCTION	7
1.1 SCOPE AND PURPOSE OF THE DOCUMENT.....	7
1.2 DEFINITIONS, ACRONYMS AND ABBREVIATIONS	7
1.3 REFERENCES.....	9
1.3.1 <i>Applicable Documents</i>	9
1.3.2 <i>Reference Documents</i>	9
2. COMPARISON OF THE PROBABILISTIC OUTPUT OF THE ASII-TF TROPopause FOLD PRODUCT USING MSG SEVIRI OR MTG FCI SATELLITE DATA 10	
2.1 VALIDATION SET-UP	11
2.2 THE FRACTIONS SKILL SCORE METHOD	12
2.3 VALIDATION OF THE ASII-TF OUTPUT WITH THE FSS METHOD	12
2.4 SUMMARY	14
3. VALIDATION OF THE MTG ASII-NG GRAVITY WAVE PRODUCT	16
4. ABOUT THE ASII-NG ICING PRODUCT, V1.0	22
5. REFERENCES	24

List of tables

Table 1: List of Applicable Documents.....	9
Table 2: List of Referenced Documents.....	9
Table 3: Central wavelength (“Central λ ”) and nominal spectral bandwidth (“ λ width”) for the MSG (SEVIRI), HIMAWARI (AHI) and MTG (FCI) channels used in ASII-TF. The nominal spectral bandwidth (μm) refers to 99% energy integrated over the channel's spectral response band.	10

List of figures

Figure 1: Comparison of the ASII-TF output with SEVIRI and FCI data for 16 January 2025 at 06:00 UTC. Highest probabilities in red and lowest probabilities in blue.	10
Figure 2: Observation (OBS) and forecast (FCST) show different patterns but the same number of hits (black squares) in the sub domain. In the shown example, FSS is 1.	11
Figure 3: Geographical area on which ASII-TF output was validated.	12
Figure 4: Exemplary plot of the FSS for combinations of thresholds (10% – 90%) applied to the ASII-TF products of 16 January 2025, 0600 UTC.	13
Figure 5: Top view on the same plot as in Figure 4	14
Figure 6: Case of 28 December 2021, 1200 UTC. Upper panel: MSG-4 IR10.8 image. Ripples characteristic for gravity waves and comparatively easily spotted in the image are present over Tunisia and the western part of the Gulf of Lion. Lower panel: The probability-of-occurrence of gravity waves, as analysed by the ASII-GW module on the basis of the IR10.8 image (the colour table runs from dark blue = 0% to red=100%).	17
Figure 7: Case of 20 December 2024, 1000 UTC. Upper panel: The probability-of-occurrence of gravity waves, as analysed by the ASII-GW module, on the basis of the MSG-4 WV7.3 ASII-GW analysis. Lower panel: Same analysis, but for the corresponding MTI-I1 image.	18
Figure 8: Case of 20 December 2024, 1000 UTC. Upper panel: The probability-of-occurrence of gravity waves, as analysed by the ASII-GW module, on the basis of the MSG-4 IR10.8 ASII-GW analysis. Lower panel: Same analysis, but for the corresponding MTI-I1 IR10.5 image.	19
Figure 9: Case of 5 December 2024, 1330 UTC. Upper panel: The probability-of-occurrence of gravity waves, as analysed by the ASII-GW module, on the basis of the MSG-4 WV7.3 ASII-GW analysis. Lower panel: Same analysis, but for the corresponding MTI-I1 image.	20
Figure 10: Case of 5 December 2024, 1330 UTC. Upper panel: The probability-of-occurrence of gravity waves, as analysed by the ASII-GW module, on the basis of the MSG-4 IR10.8 ASII-GW analysis. Lower panel: Same analysis, but for the corresponding MTI-I1 IR10.5 image.	21
Figure 11: Case of 20 December 2024, 1000 UTC. Upper panel: ASII-ICE High-Altitude Ice Crystals product, MSG-4. Lower panel: Same analysis, but for the corresponding MTG –FCI input.	22
Figure 12: Case of 20 December 2024, 1000 UTC. Upper panel: ASII-ICE icing-due-to-supercooled-water-droplets product, MSG-4. Lower panel: Same analysis, but for the corresponding MTG –FCI input.	23

1. INTRODUCTION

EUMETSAT’s “Satellite Application Facilities” (SAFs) are dedicated centres of excellence for processing satellite data, and form an integral part of the distributed EUMETSAT Application Ground Segment (<http://www.eumetsat.int>). This documentation is provided by the SAF on Support to Nowcasting and Very Short-Range Forecasting, NWC SAF. The main objective of NWC SAF is to provide, further develop and maintain software packages to be used for Nowcasting applications of operational meteorological satellite data by National Meteorological Services. More information can be found at the NWC SAF webpage, <http://www.nwc-saf.eumetsat.int>.

1.1 SCOPE AND PURPOSE OF THE DOCUMENT


This document is the Validation Report for the NWC/GEO Automatic Satellite Interpretation – Next Generation Product (PGE17, ASII-NG), NWC/GEO release 2025, comprised of ASII-TF (tropopause fold detection sub-product), v3.0 (chapter 2), ASII-GW (gravity wave detection sub-product), v2.0 (chapter 3), and ASII-ICE (in-flight icing sub-product), v1.0 (chapter 4).

This document contains a description of the validation method and the corresponding results for ASII-TF. Concerning ASII-GW and ASII-ICE, it shows a few examples contrasting MSG and MTG outcome demonstrating the continuity of the products.

1.2 DEFINITIONS, ACRONYMS AND ABBREVIATIONS

AHI	Advanced Himawari Imager
ASII	Automatic Satellite Image Interpretation
ASII-GW	Gravity wave detection sub-product of ASII-NG
ASII-NG	Automatic Satellite Image Interpretation – Next Generation
ASII-TF	Tropopause fold detection sub-product of ASII-NG
ATBD	Algorithm Theoretical Baseline Document
EUMETSAT	European Organisation for the Exploitation of Meteorological Satellites
FCI	Flexible Combined Imager
FSS	Fractions Skill Score
GW	Gravity wave(s)
IR	Infrared
MSG	Meteosat Second Generation
MTG	Meteosat Third Generation
NRT	Near-Real Time
NWCSAF	SAF to support NoWCasting and Very-Short-Range Forecasting
NWP	Numerical Weather Prediction

PGE	Product Generation Element
SAF	Satellite Application Facility
SEVIRI	Spinning Enhanced Visible and Infrared Imager
UTC	Universal Time Coordinated
WV	Water Vapour

	Scientific and Validation Report for the “Automatic Satellite Image Interpretation – Next Generation” Processors of the NWC/GEO	Code: NWC/CDOP4/MTG/GSA/SCI/VR/ASII-NG Issue: 1.0.0 Date: 31 March 2025 File: NWC-CDOP4-MTG-GSA-SCI-VR-ASII-NG_v1.0.0 Page: 9/24
---	--	--

1.3 REFERENCES

1.3.1 Applicable Documents

The following documents, of the exact issue shown, form part of this document to the extent specified herein. Applicable documents are those referenced in the Contract or approved by the Approval Authority. They are referenced in this document in the form [AD.X].

For dated references, subsequent amendments to, or revisions of, any of these publications do not apply. For undated references, the current edition of the document referred applies.

Current documentation can be found at the NWC SAF Helpdesk web: <http://www.nwc-saf.eumetsat.int>.

Ref	Title	Code	Vers	Date
[AD.1]	Proposal for the Fourth Continuous Development and Operations Phase (CDOP 4) March 2022 – February 2027	/NWC/SAF/AEMET/MGT/CDOP4Proposal	1.0	12/03/2021
[AD.2]	Project Plan for the NWCSAF CDOP4 phase	NWC/CDOP4/SAF/AEMET/MGT/PP	3.0.0	21/10/2024
[AD.3]	Configuration Management Plan for the NWCSAF	NWC/CDOP4/SAF/AEMET/MGT/CMP	1.2.0	29/03/2024
[AD.4]	NWCSAF Product Requirement Document	NWC/CDOP4/SAF/AEMET/MGT/PRD	3.0.0	21/10/2024
[AD.5]	NWCSAF CDOP 4 Service Specifications	NWC/CDOP4/SAF/AEMET/MGT/SSD	1.0.0	31/10/2022
[AD.6]	System and Components Requirements Document for the NWC/GEO MTG-I day-1	NWC/CDOP2/MTG/AEMET/SW/SCRD	1.3.1	31/03/2025
[AD.7]	Architecture Design Document for the NWC/GEO MTG-I day-1	NWC/CDOP2/MTG/AEMET/SW/ACDD	1.3.0	31/03/2025
[AD.8]	Interface Control Document for Internal and External Interfaces of the NWC/GEO MTG-I day-1	NWC/CDOP2/MTG/AEMET/SW/ICD/1	1.4.0	31/03/2025
[AD.9]	Interface Control Document for the NWCLIB of the NWC/GEO MTG-I day-1	NWC/CDOP2/MTG/AEMET/SW/ICD/2	1.4.0	31/03/2025
[AD.10]	Data Output Format for the NWC/GEO MTG-I day-1	NWC/CDOP2/MTG/AEMET/SW/DOF	1.4.0	31/03/2025
[AD.11]	User Manual for the NWC/GEO: Software Part	NWC/CDOP3/MTG/AEMET/SW/UM	1.3.0	31/03/2025

Table 1: List of Applicable Documents

1.3.2 Reference Documents

The reference documents contain useful information related to the subject of the project. These reference documents complement the applicable ones, and can be looked up to enhance the information included in this document if it is desired. They are referenced in this document in the form [RD.X].

For dated references, subsequent amendments to, or revisions of, any of these publications do not apply. For undated references, the current edition of the document referred applies.

Current documentation can be found at the NWC SAF Helpdesk web: <http://www.nwc-saf.eumetsat.int>.

Ref	Title	Code	Vers	Date
[RD.1]	The Nowcasting SAF Glossary	NWC/CDOP4/SAF/AEMET/MGT/GLO	1.0.0	31/10/23
[RD.2]	User Manual for the “Automatic Satellite Image Interpretation – Next Generation” Processors of the NWC/GEO: Science Part	NWC/CDOP3/MTG/ZAMG/SCI/UM/ASI-I-NG	1.2.0	31/05/25
[RD.3]	Algorithm Theoretical Baseline Document for the “Automatic Satellite Image Interpretation – Next Generation” Processor of the NWC/GEO	NWC/CDOP2/MTG/ZAMG/SCI/ATBD/ASII-NG	1.1.1	31/05/25
[RD.4]	Scientific and Validation Report for the “Automatic Satellite Image Interpretation – Next Generation” Processors of the NWC/GEO	NWC/CDOP3/GEO/ZAMG/SCI/VR/ASII-NG	1.0	21/01/19

Table 2: List of Referenced Documents

2. COMPARISON OF THE PROBABILISTIC OUTPUT OF THE ASII-TF TROPOPAUSE FOLD PRODUCT USING MSG SEVIRI OR MTG FCI SATELLITE DATA

The ASII-TF product provides probability values [0-100%] for the presence of a tropopause fold for each pixel of the geostationary satellite image.

The product was originally developed using Meteosat Second Generation (MSG) SEVIRI data in combination with ECMWF model data. By applying the logistic regression method, weighting coefficients were derived for the specific input parameters. When technically adapting ASII-TF for Meteosat Third Generation (MTG) FCI data, coefficients derived for the HIMAWARI AHI proxy were used. Table 3 shows the characteristics of the involved channels.

MSG SEVIRI		HIMAWARI AHI		MTG FCI	
Central λ (μm)	λ width (μm)	Central λ (μm)	λ width (μm)	Central λ (μm)	λ width (μm)
WV 6.25	1.80	WV 6.24	0.37	WV 6.30	1.00
IR 9.66	0.56	IR 9.64	0.18	IR 9.66	0.30
IR 10.8	2.0	IR 10.40	0.30	IR 10.50	0.70

Table 3: Central wavelength (“Central λ ”) and nominal spectral bandwidth (“ λ width”) for the MSG (SEVIRI), HIMAWARI (AHI) and MTG (FCI) channels used in ASII-TF. The nominal spectral bandwidth (μm) refers to 99% energy integrated over the channel’s spectral response band.

The validation of the ASII-TF product consisted in a comparison between the product based on SEVIRI data (ASII-TF SEVIRI) and the one using FCI satellite data (ASII-TF FCI). A visual inspection of both product outputs shows a good agreement regarding the position of the tropopause folds and the indicated probability values (**Figure 1**).

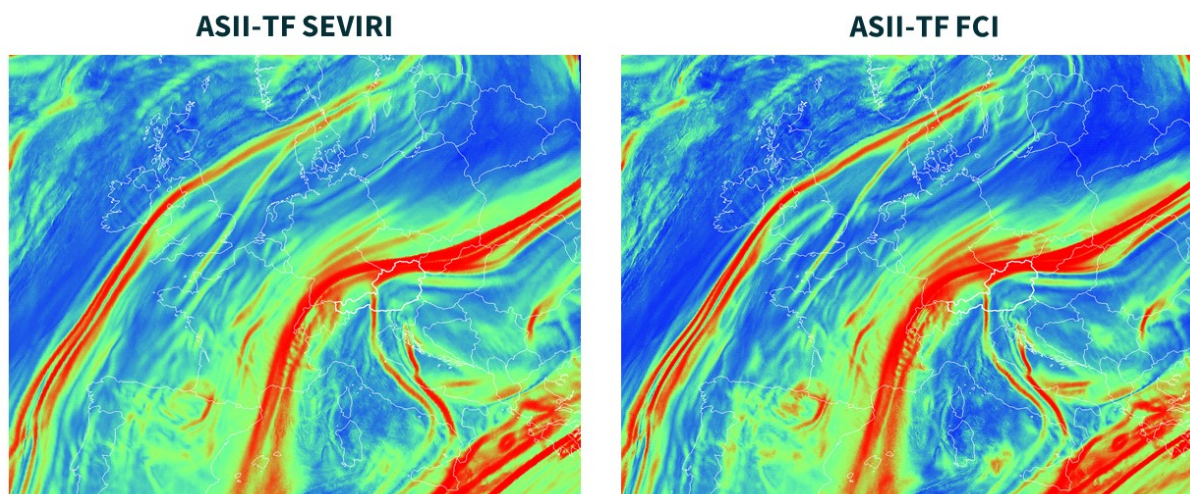


Figure 1: Comparison of the ASII-TF output with SEVIRI and FCI data for 16 January 2025 at 06:00 UTC. Highest probabilities in red and lowest probabilities in blue.

To obtain a quantitative estimation of the deviation, the concept of the Fractions Skill Score (FSS) was applied. The Fractions Skill Score is a spatial verification metric routinely computed in operational verification suites. It assumes 1 for a perfect fit and is 0 for a complete miss. Any value

of the FSS below 0.5 can be considered as “no skill”. The FSS method was initially developed to compare forecast and observation of precipitation fields by setting a precipitation threshold in a sub-grid domain for which the pattern of the precipitation maxima does not matter as long as the precipitation covers the same area share in the sub-domain (see **Figure 2**).

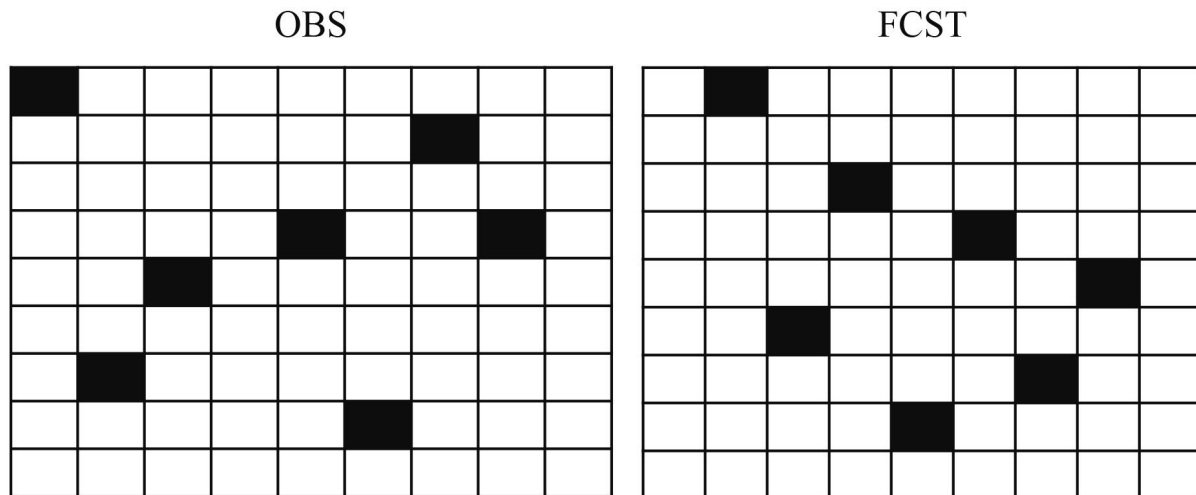


Figure 2: Observation (OBS) and forecast (FCST) show different patterns but the same number of hits (black squares) in the sub domain. In the shown example, FSS is 1.

The results of the FSS depend on two parameters:

1. The size of the sub-domain, which defines a maximum permissible spatial shift between reference and test field
2. The threshold applied to the parameter, e.g. ASII-TF probability > 80%. Values above the threshold are counted as a "hit".

The FSS method can be applied to fields with different horizontal resolutions, as it is the case with the two sensors, for as long as the same sub-domain is compared.

2.1 VALIDATION SET-UP

The period during which the results of ASII-TF were compared extends from 10 October 2024 to 20 January 2025, and includes 16 data sets. Each data set consisted of the ASII-TF analysis using SEVIRI data and the corresponding results of ASII-TF based on FCI satellite data. To obtain a temporally corresponding output from the two data sources, results were chosen either on the hour or on the half-hour (SEVIRI has a 15-minutes scan interval, FCI 10). The validation dataset is dominated by winter cases.

The evaluation was done for the same region (**Figure 3**) comprising 1100x650 pixel for SEVIRI and 1650x974 pixel for FCI.



Figure 3: Geographical area on which ASII-TF output was validated.

2.2 THE FRACTIONS SKILL SCORE METHOD

The Fractions Skill Score (FSS) method was introduced by Roberts and Lean in 2008 and has shown good practicability for validating precipitation forecasts which often suffer from the double penalty problem of being either predicted at the wrong location or time. This method is best suited for comparing forecasts and analyses with different horizontal resolution as in our validation example. In order to validate the output of ASII-TF, the output of ASII-TF using SEVIRI image data was considered as ‘truth’.

The fractions skill score is a neighbourhood verification method originally designed to verify deterministic forecasts of binary events. This is in the present case the fraction of pixels exceeding a threshold (called ‘hits’) for both the reference data (ASII-TF SEVIRI) and the product to be validated (ASII-TF FCI). The location of the hits does not play a role as long as the hit is located inside the same sub-domain. Therefore, two essential parameters have to be defined beforehand: the size of the sub-areas (also: window size or neighbourhood) and the threshold for defining a hit.

Typically, the FSS is computed for a range of window sizes and the resulting score plotted as a function of window size. This allows determining the scale at which the FSS reaches the target skill of

$$FSS_{target} = 0.5 + \frac{f}{2} \quad [Eq. 1]$$

(Faggian et al., 2015), where f is the fractional ‘hit’ coverage over the validation area (hit-area ratio). If f is not very large (within a large domain), a value of 0.5 can be used as a lower limit, and then skillfulness can be assumed for $FSS \geq 0.5$ (Zhao and Zhang, 2018).

2.3 VALIDATION OF THE ASII-TF OUTPUT WITH THE FSS METHOD

As mentioned above, two parameters have to be defined beforehand:

1. A threshold that distinguishes a hit from a miss

2. The size of the sub-domain

Regarding point 1:

For both ASII-TF products, the applied thresholds characterizing a hit was varied from 10% to 90% in increments of 1%, which results in $81^2 = 6561$ Fractions Skill Scores for every test case sample. The highest FSS values are expected for equivalent thresholds for both products in case of a similar output.

Regarding point 2:

The size of the sub-domain was chosen as 50 by 50 pixels for ASII-TF SEVIRI and 75 by 75 pixels for ASII-TF FCI, accounting for the different horizontal resolutions of the two sensors. No other sub-domain size was tested during the validation.

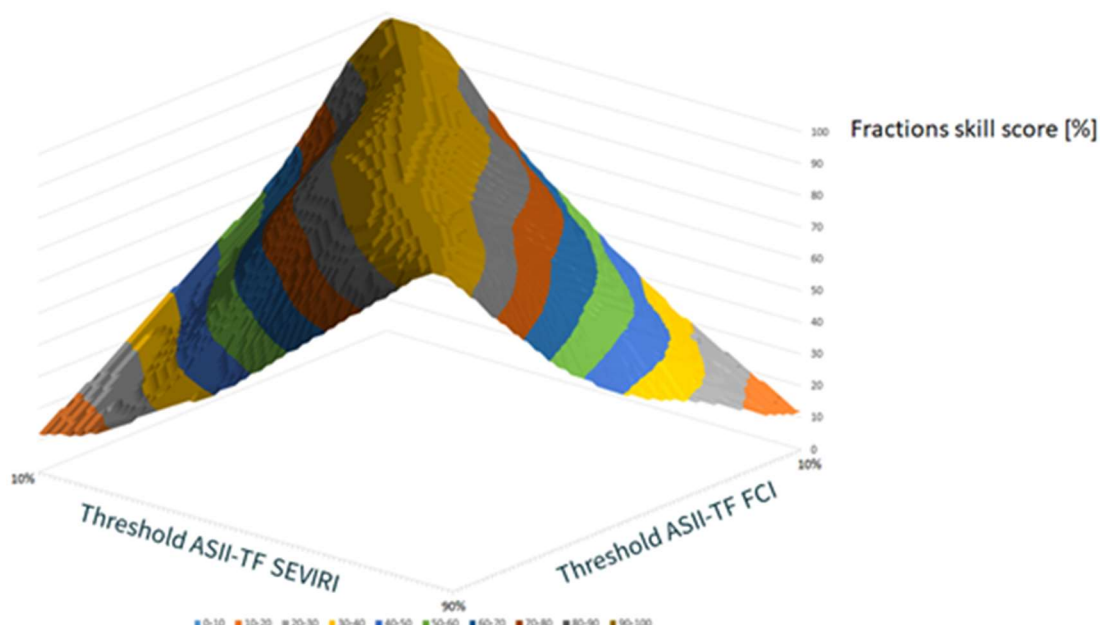


Figure 4: Exemplary plot of the FSS for combinations of thresholds (10% – 90%) applied to the ASII-TF products of 16 January 2025, 0600 UTC. Colors used to reflect the value of the FSS (0 – 100%) even more clearer.

For all investigated cases, the FSS diagrams look almost identical: the highest FSS values were obtained for similar probability thresholds of ASII-TF SEVIRI and ASII-TF FCI. The more the probability thresholds diverge, the lower the FSS, as seen in a slope on both sides of the 3-D FSS plot (see **Figure 4**). The result is in agreement with the expectation to obtain a similar output when applying similar thresholds to the two compared products.

However, a change of the perspective reveals a minor deviation of the line of highest FSS (black line in **Figure 5**) from the line of the perfect fit where the highest FSS are located along the line of equivalent thresholds (i.e., the red line in **Figure 5**). A perfect fit would show a uniform gradient on both sides of the red line with color bands running in parallel to the red line.

The results also indicate that no significant horizontal shifts in the ASII-TF results are observed as the highest Fraction Skill Scores show 100% agreement along the line of equal thresholds (**Figure 5**).

The black line corresponds to the ridge of the FSS topography and reflects the thresholds for ASII-TF SEVIRI and ASII-TF FCI that provide the best fit (i.e. highest FSS). The red line corresponds to the line of equal thresholds in both product outputs and represents the ideal scenario where best fit is achieved. A slight bias of the black line to the right can be observed for lower ASII-TF probabilities and a slightly stronger bias to the left for higher ASII-TF probabilities.

This bias can be interpreted as follows:

- **For higher ASII-TF probability values** (lower corner of the graph in *Figure 5*), best-matching results are found with slightly higher probability thresholds of ASII-TF FCI. This means that ASII-TF FCI shows slightly higher values than ASII-TF SEVIRI in areas where a tropopause fold is detected.
- **For lower ASII-TF probability values** (upper corner of the graph in *Figure 5*), best matching results are found with slightly lower probability thresholds of ASII-TF FCI. This means that ASII-TF FCI shows slightly lower values than ASII-TF SEVIRI in areas without a tropopause fold.

For all cases in the evaluation period, this bias is not very strong, barely noticeable when visually comparing both product outputs but manifest in a quantitative comparison of the whole dataset. The observed bias is independent from daytime and no other trend was observed in the four-month data set (October 2024 to January 2025).

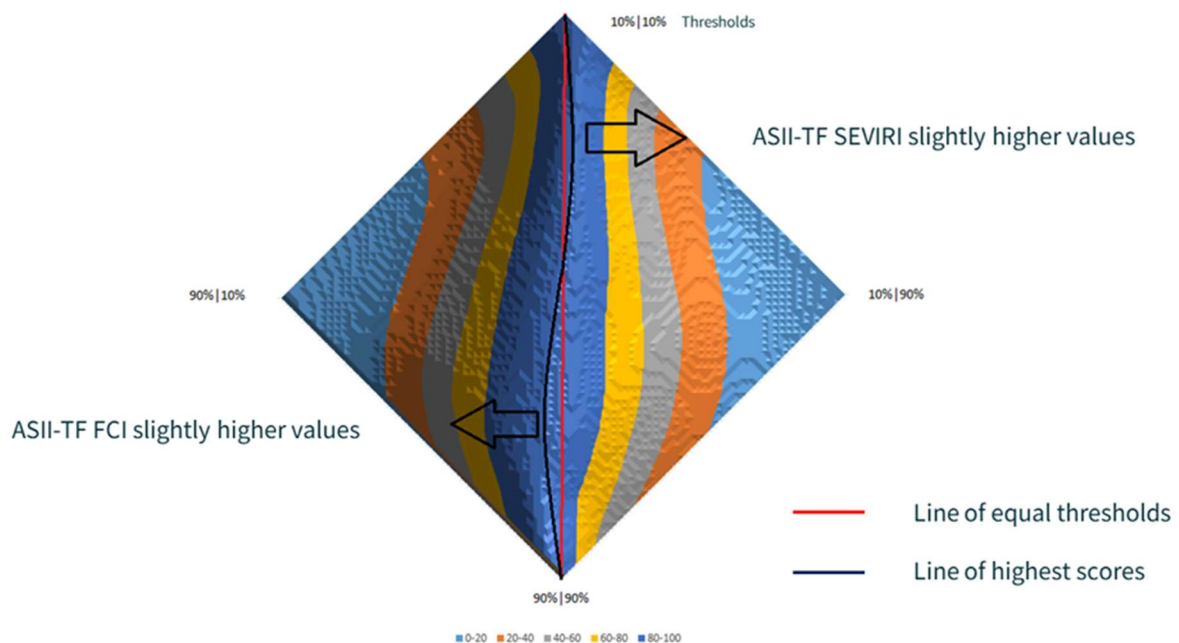



Figure 5: Top view on the same plot as in Figure 4.

2.4 SUMMARY

The aim of this investigation was to find out how the ASII-TF product output changes when using the novel satellite data from Meteosat Third Generation instead of the MSG SEVIRI data that was used to develop the product. Compared to MSG SEVIRI channels, MTG FCI satellite channels differ in central wavelengths, spectral widths and spatial resolutions.

	Scientific and Validation Report for the “Automatic Satellite Image Interpretation – Next Generation” Processors of the NWC/GEO	Code: NWC/CDOP4/MTG/GSA/SCI/VR/ASII-NG Issue: 1.0.0 Date: 31 March 2025 File: NWC-CDOP4-MTG-GSA-SCI-VR-ASII-NG_v1.0.0 Page: 15/24
---	--	---

The eyeball verification shows a good agreement between both products when using the same NWP input data (ECMWF) but different satellite data for all investigated cases in the period from October 2024 to January 2025.

A quantitative comparison of the two products was done with help of the FSS method. The method confirmed the good agreement of the probability values for both products using either SEVIRI or FCI input data, but also revealed out minor differences. In the higher probability range (70% to 90% probability for a tropopause fold) ASII-TF FCI shows slightly higher probability values compared to ASII-TF SEVIRI (for the lower probabilities (10% to 30%), the relation is numerically reversed, but the absolute value is actually insignificant for meteorological interpretation in this range).

Given the good agreement between ASII-TF FCI probabilities and those from ASII-TF SEVIRI, it is justified to use FCI satellite data as input for ASII-TF with AHI-derived coefficients for the time being. Of course, as AHI is not a 100% perfect proxy for FCI (cf. Table 3), it is still advisable to derive coefficients from actual FCI data as soon as enough data over the whole annual cycle are available.

3. VALIDATION OF THE MTG ASII-NG GRAVITY WAVE PRODUCT

As described in the ATBD [RD.3], the ASII-NG product suite will include modules relevant for aviation meteorology, enabling the objective detection of patterns commonly associated with (clear-air) turbulence. The idea behind the ASII-NG gravity wave product (ASII-GW) is to support the aviation forecasters in making their decision more quickly by relieving them from a subjective search over the whole image by providing a reliable objective identification of the relevant pattern. In the case of ASII-GW, the relevant signal observed in satellite imagery consists of parallel stripes / ripples (see **Figure 6**). As concluded in the general discussion in the validation report [RD.4], the scope of ASII-GW validations is to assess how well the results of the employed pattern recognition algorithm align with a subjective diagnosis of these patterns. This has been proven in [RD.4] for MSG. The nature of the product/algorithm makes it straightforward to adapt the input with increased spatial resolution. He et al. (2020) explored the application of the algorithm to the higher-resolution AHI data from Himawari (with a spatial resolution practically identical to FCI) and confirmed the adequacy of the algorithmic parameters, which were adapted based on the ratio of pixel sizes of the sensors. Nevertheless, to be on the safe side, the product was also examined during the first months of FCI reception to verify its comparability with the MSG counterpart.

We built a collection of cases in the fourth quarter of 2024. From these cases, selected randomly in NRT when time permitted and sufficient signals were observed in one of the analysed channels, we have chosen those with the highest number of gravity wave signals. These selected cases thus feature multiple instances of the phenomenon within one image.

The case of 20 December 2024, 10 UTC, is chosen here as the most relevant one for the WV7.3 channel, with many “classical” places (Algeria/Tunisia, Southern France, Southern Italy) showing gravity wave signals (**Figure 7**). Clearly, the gravity wave analyses show essentially the same features for MSG and MTG, with the “red”/alert regions often with slightly higher extension for MTG. This could be due to the higher-resolving capabilities of the FCI capturing weaker signals at the edge of the striped areas somewhat better. Comparing the IR 10.8 analyses (**Figure 8**) yields a similar impression (they are included here for the sake of completeness though the channel is clearly less relevant for this case than the WV 7.3 channel).

Moving to the case of 5 December 2024, 1330 UTC, one can say about the WV7.3 analyses in **Figure 9** little more than the picture confirms what was already said about **Figure 7**. But concerning the IR analyses, we considered this as the most interesting of the inspected cases: By and large, the prominent signals appear in the same regions for MSG and MTG (as well as in the same regions observed in the WV images), **Figure 10**. There is a very weak signal for MSG in central Germany, which is a bit more pronounced in MTG; the converse is true for signals at the border Croatia-Serbia. Probably this shows how, on the scale of gravity waves, the relative position of the pattern to the image pixels impacts the strength of the signal. Yet, in essence, it is also evidence that even for such weak signals there is nothing one could call a disruption, when going from MSG to MTG.

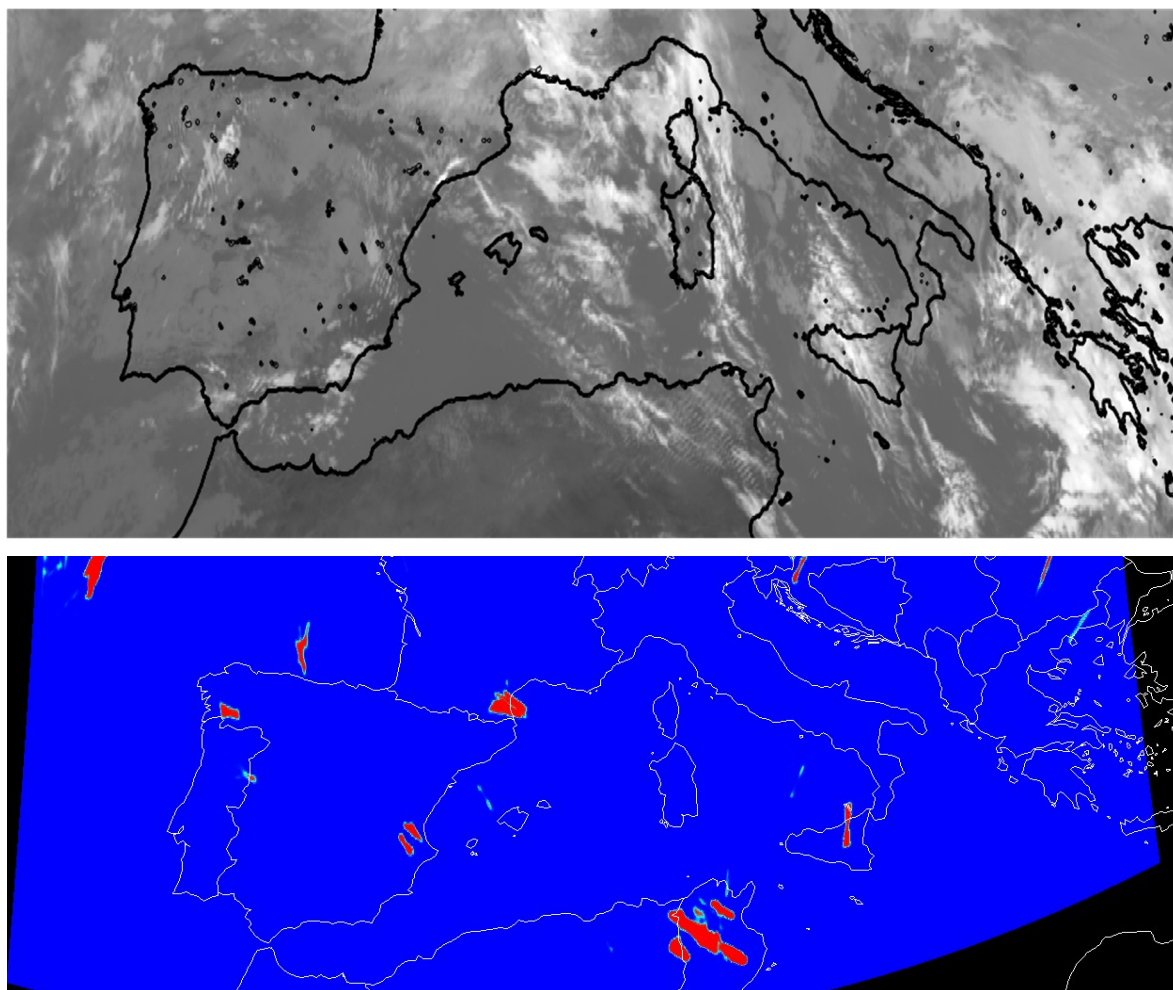


Figure 6: Case of 28 December 2021, 1200 UTC. Upper panel: MSG-4 IR10.8 image. Ripples characteristic for gravity waves and comparatively easily spotted in the image are present over Tunisia and the western part of the Gulf of Lion. Lower panel: The probability-of-occurrence of gravity waves, as analysed by the ASII-GW module on the basis of the IR10.8 image (the colour table runs from dark blue = 0% to red=100%).

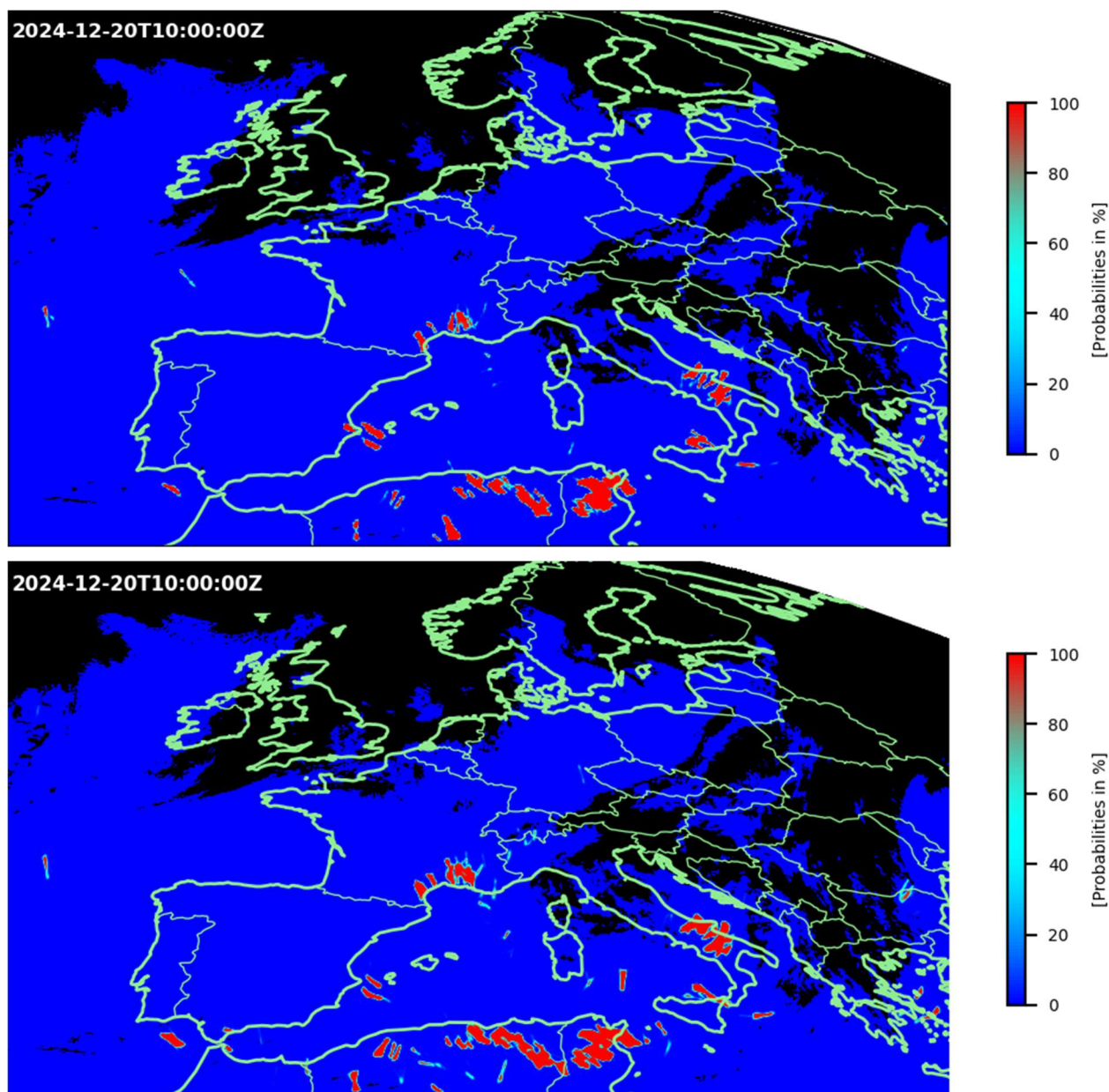


Figure 7: Case of 20 December 2024, 1000 UTC. Upper panel: The probability-of-occurrence of gravity waves, as analysed by the ASII-GW module, on the basis of the MSG-4 WV7.3 ASII-GW analysis. Lower panel: Same analysis, but for the corresponding MTI-II image.

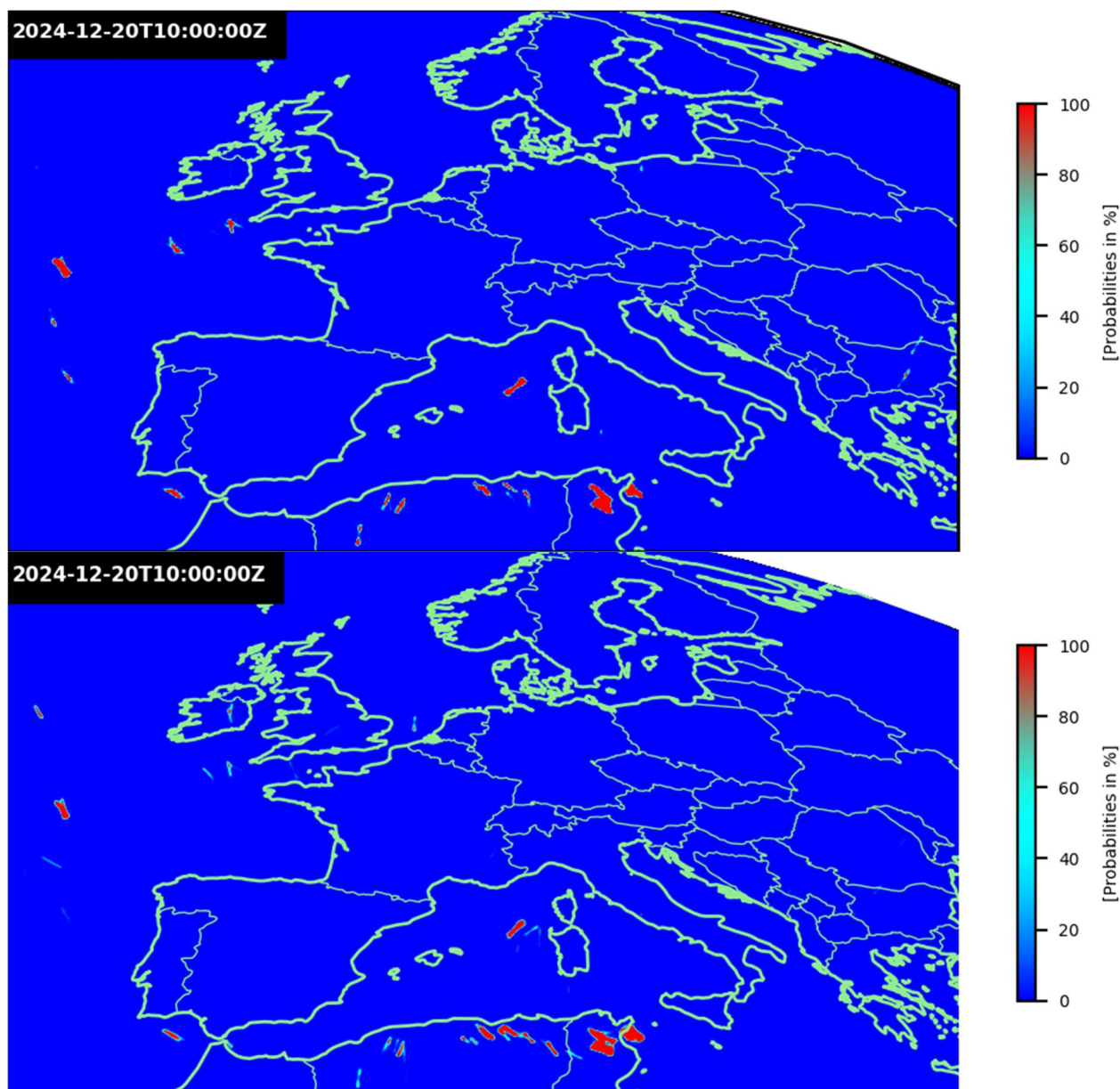


Figure 8: Case of 20 December 2024, 1000 UTC. Upper panel: The probability-of-occurrence of gravity waves, as analysed by the ASII-GW module, on the basis of the MSG-4 IR10.8 ASII-GW analysis. Lower panel: Same analysis, but for the corresponding MTI-II IR10.5 image.

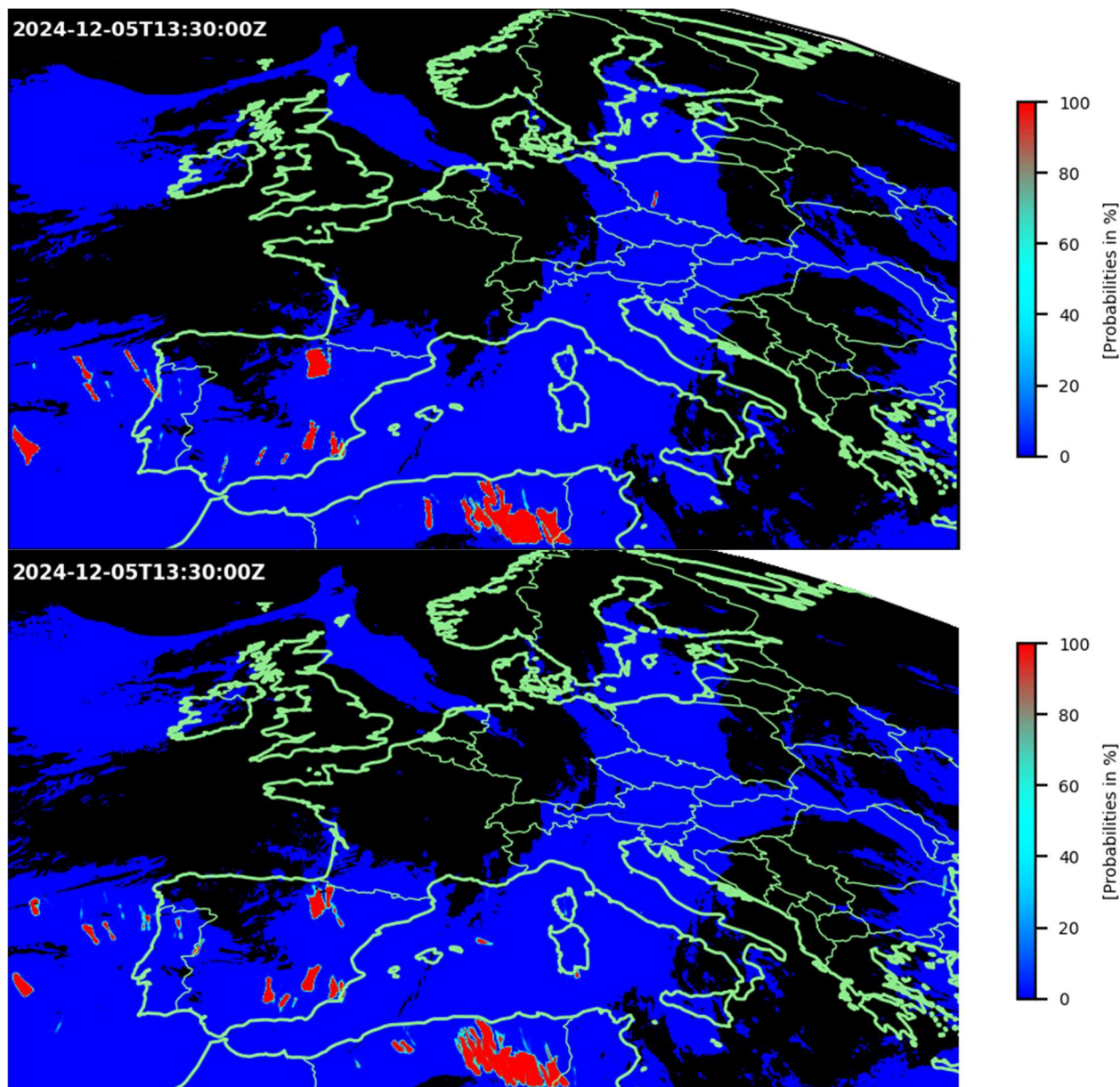


Figure 9: Case of 5 December 2024, 1330 UTC. Upper panel: The probability-of-occurrence of gravity waves, as analysed by the ASII-GW module, on the basis of the MSG-4 WV7.3 ASII-GW analysis. Lower panel: Same analysis, but for the corresponding MTI-II image.

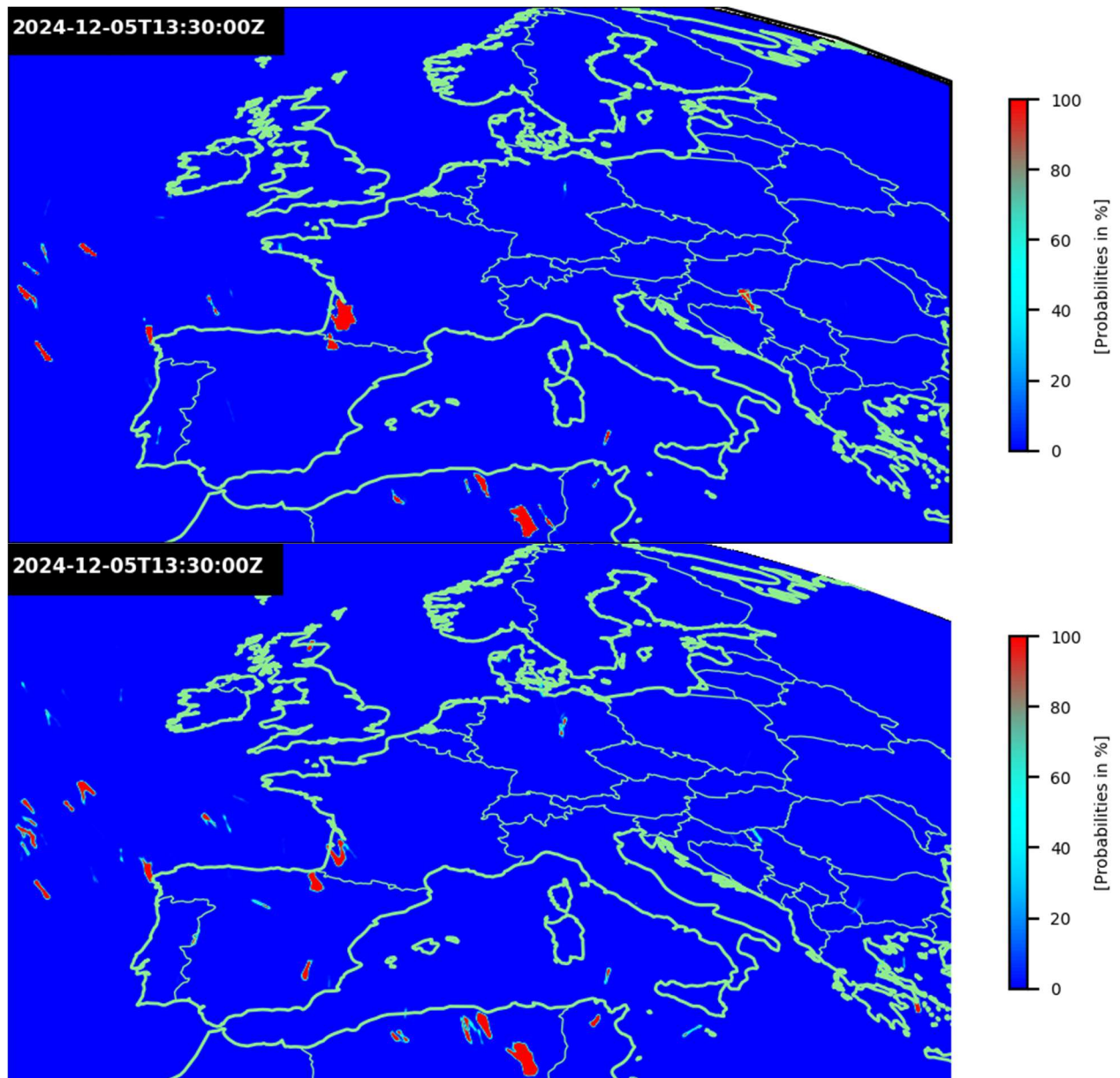


Figure 10: Case of 5 December 2024, 1330 UTC. Upper panel: The probability-of-occurrence of gravity waves, as analysed by the ASII-GW module, on the basis of the MSG-4 IR10.8 ASII-GW analysis. Lower panel: Same analysis, but for the corresponding MTI-II IR10.5 image.

4. ABOUT THE ASII-NG ICING PRODUCT, V1.0

In its first version (with demonstrational status), the in-flight icing product provides a direct implementation of two established approaches—supercooled water hazard detection (Smith et al., 2012) and high-altitude ice crystal hazard detection (de Laat et al., 2017). By doing so, it makes these methodologies available as a dataset to the NWC/GEO community, both of which have demonstrated value through validation campaigns.

The two sub-products are based solely on CTTH and CMIC input; consequently, if the Nowcasting-SAF products CTTH and CMIC have continuity between the MSG era and the MTG era, so have the ASII-ICE products. In this sense, the respective MTG Validation Reports of the two input products implicitly cover the case of ASII-ICE as well. Nevertheless, we dumped the ASII-ICE products together with the ASII-GW products in the validation campaign discussed in the previous chapter, and for illustrative purposes include here the case of 20 December 2024, 1000 UTC (**Figure 11, Figure 12**). Note there is currently no night-time mode for these products, so the inspection of wintertime cases over Europe obviously has its limitations, but what we see in the images gives no reasons for concern.

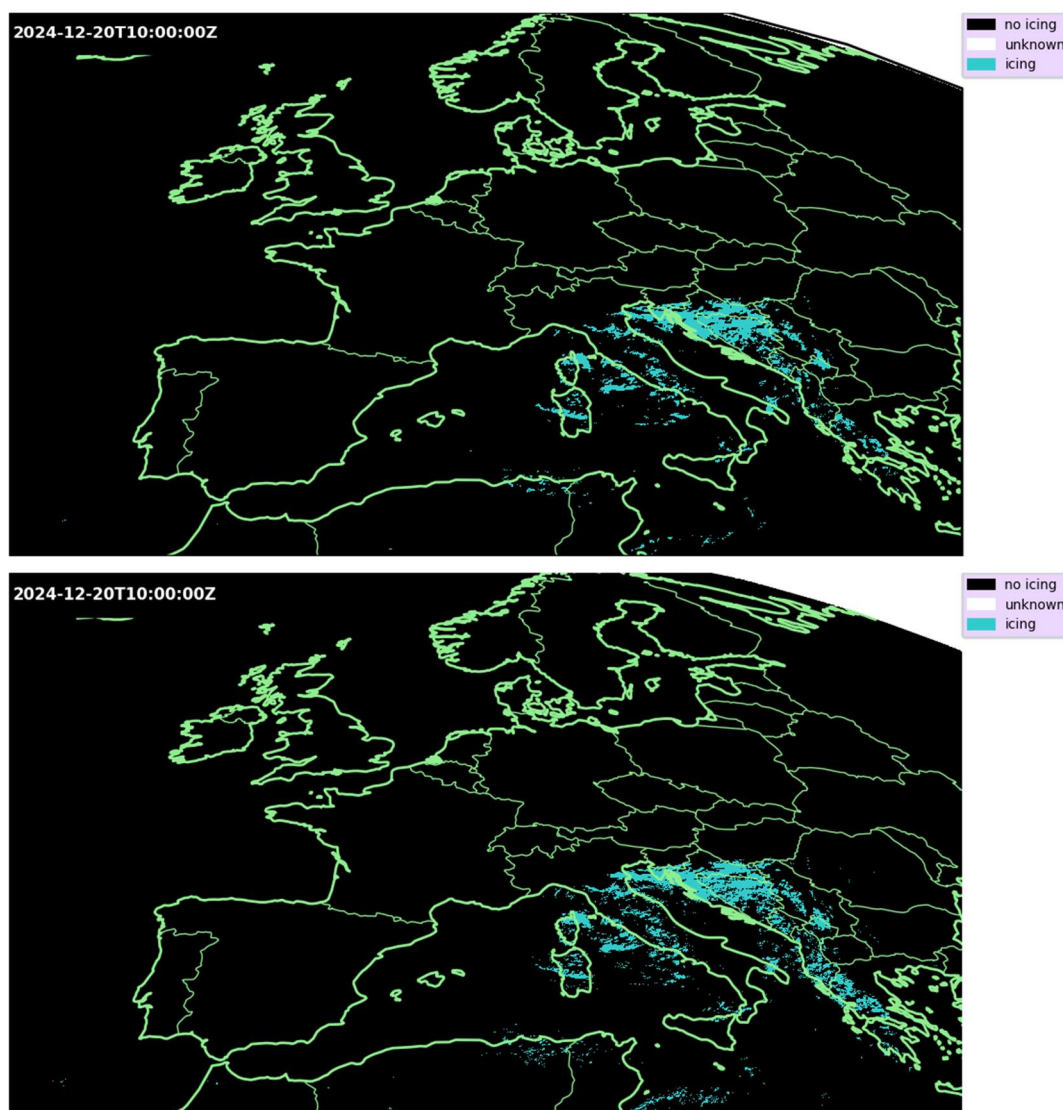


Figure 11: Case of 20 December 2024, 1000 UTC. Upper panel: ASII-ICE High-Altitude Ice Crystals product, MSG-4. Lower panel: Same analysis, but for the corresponding MTG-FCI input.

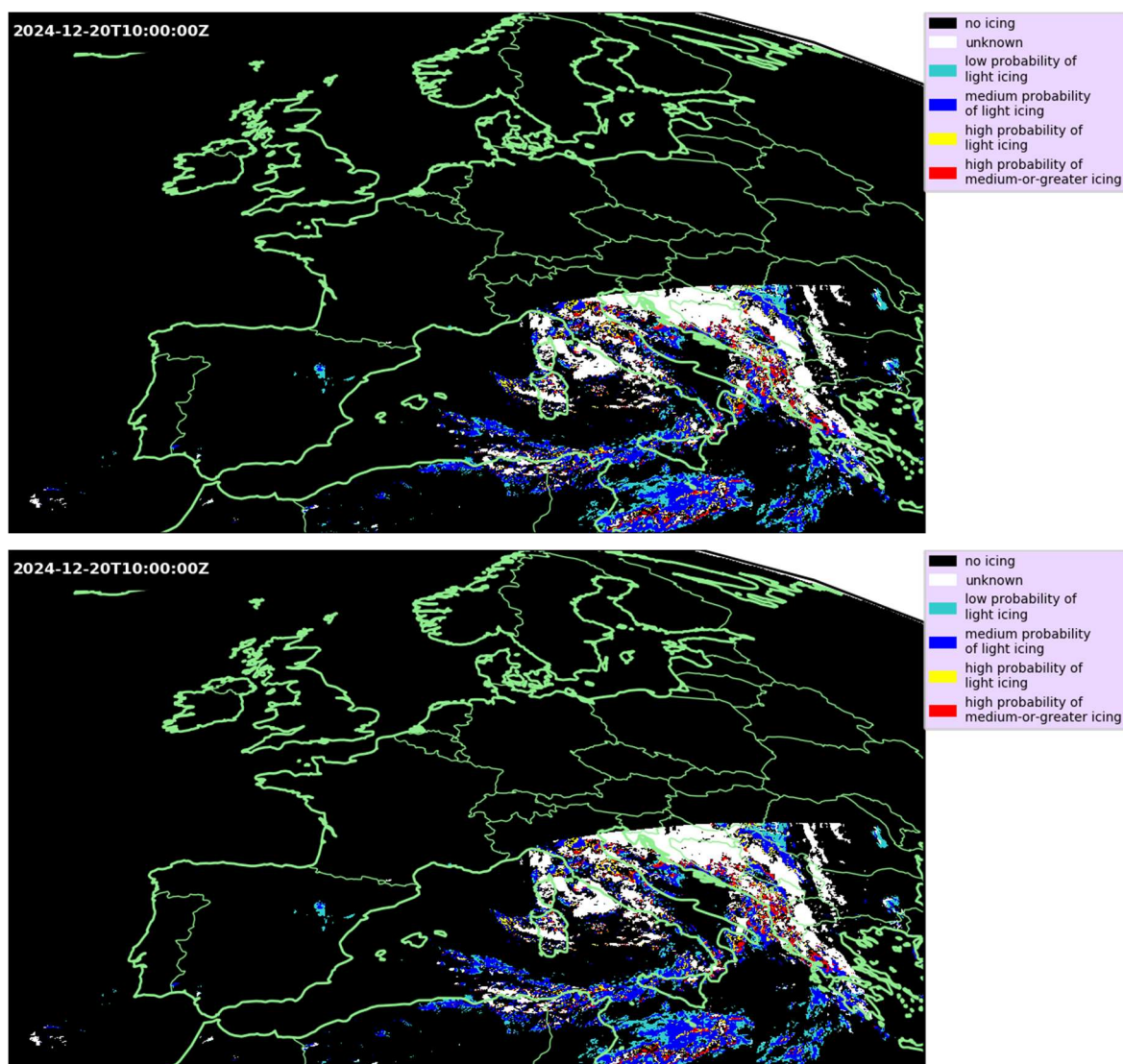


Figure 12: Case of 20 December 2024, 1000 UTC. Upper panel: ASII-ICE icing-due-to-supercooled-water-droplets product, MSG-4. Lower panel: Same analysis, but for the corresponding MTG –FCI input.

5. REFERENCES

- de Laat, A., Defer, E., Delanoë, J., Dezitter, F., Gounou, A., Grandin, A., Guignard, A., Meirink, J. F., Moisselin, J.-M., and Parol, F. (2017): Analysis of geostationary satellite-derived cloud parameters associated with environments with high ice water content. *Atmos. Meas. Tech.*, **10**, 1359-1371, <https://doi.org/10.5194/amt-10-1359-2017>.
- Faggian, N., B. Roux, P. Steinle and B. Ebert (2015): Fast calculation of the fractions skill score. *Mausam*, **66**, 457-466.
- He, N., A. Jann and Y. Wang (2020): Objective detection of gravity waves in Himawari-8 imagery in support of aviation forecasting. *Meteorol. Z. (Contrib. Atm. Sci.)*, **29**, 323–332.
- Roberts, N.M., and H.W. Lean (2008): Scale-selective verification of rainfall accumulations from high-resolution forecasts of convective events. *Mon. Wea. Rev.*, **136**, 78–97.
- Smith W. L., Jr., P. Minnis, C. Fleege, D. Spangenberg, R. Palikonda, and L. Nguyen (2012): Determining the flight icing threat to aircraft with single-layer cloud parameters derived from operational satellite data. *J. Appl. Met. Climatol.*, **51**, 1794-1810.
- Zhao, B., and B. Zhang (2018): Assessing hourly precipitation forecast skill with the Fractions Skill Score. *J. Meteor. Res.*, **32**, 135-145, <https://doi.org/10.1007/s13351-018-7058-1>.